Check for updates

OPEN

Suppression of surface ozone by an aerosol-inhibited photochemical ozone regime

Peter D. Ivatt[1,2], Mathew J. Evans [ID][1,2 ✉] and Alastair C. Lewis [ID][1,2]

Atmospheric ozone (O_3) is a pollutant produced through chemical chain reactions where volatile organic compounds (VOCs), carbon monoxide and methane are oxidized in the presence of oxides of nitrogen (NO_x). For decades, the controlling chain termination step has been used to separate regions into either 'NO_x limited' (peroxyl-radical self-reactions dominate) or 'VOC limited' (hydroxyl radical (OH) + nitrogen dioxide (NO_2) reaction dominates). The controlling regime would then guide policies for reducing emissions and so O_3 concentrations. Using a chemical transport model, we show that a third 'aerosol inhibited' regime exists, where reactive uptake of hydroperoxyl radicals (HO_2) onto aerosol particles dominates. In 1970, 2% of the Northern Hemisphere population lived in an aerosol-inhibited regime, but by 2014 this had increased to 21%; 60% more than lived in a VOC-limited regime. Aerosol-inhibited chemistry suppressed surface O_3 concentrations in North America and Europe in the 1970s and is currently suppressing surface O_3 over Asia. This third photochemical O_3 regime leads to potential trade-off tensions between reducing particle pollution in Asia (a key current health policy and priority) and increasing surface O_3, should O_3 precursors emissions not be reduced in tandem.

Ozone (O_3) has well-documented detrimental impacts on human and ecosystem health, and in the mid to upper free troposphere is a greenhouse gas[1,2]. Since the mid-twentieth century, it has been known that O_3 is formed through complex radical chain-reaction chemistry involving the oxidation of volatile organic compounds (VOCs) in the presence of oxides of nitrogen (NO_x) (ref. [3]). The chain reaction is initiated through the photolysis of photo-labile compounds such as O_3, CH_2O and HONO, propagated through the interconversion of peroxyl (HO_2 and RO_2) and hydroxyl (OH) radicals and terminated either through the self-reaction of peroxyl radicals to form longer-lived species (such as peroxides) or from the reaction of a hydroxyl radical with nitrogen dioxide (NO_2) to form nitric acid (HNO_3)[4,5]. From the perspective of reducing O_3 pollution, the dominant termination step is often used to identify whether reductions in the emissions of NO_x or VOCs should be preferentially employed[6]. If peroxyl-radical self-reactions dominate (known as the 'NO_x limited' regime), reductions in NO_x emissions are most beneficial, whereas if the NO_2 + OH reaction dominates (known as the 'VOC limited' regime) reductions in organic emissions are most effective. The existence of these two well-defined O_3 production regimes has been used to guide national-, regional- and city-level air-quality policy choices for many decades[3].

Since the development of the NO_x- versus VOC-limited model, understanding of atmospheric chemistry has advanced, with increased understanding of VOC chemistry[7], aerosols[8], halogens[9] and so on. In this study, we use a chemistry transport model with an advanced representation of atmospheric chemistry (GEOS-Chem[10]) to diagnose the balance of termination steps. Notably, the model includes the uptake of HO_2 onto aerosol surfaces, which has been identified as an important process for chain termination over the past decades[8,11–15]. We compare the rate of radical termination by peroxyl-radical self-reactions, the OH + NO_2 reaction and the uptake of HO_2 onto aerosol in July for the Northern Hemisphere in the pre-industrial era (1750), 1970 and 2014 (Methods).

Concentrations of key components calculated by the model are shown in Supplementary Figs. 1–6.

Chain termination

Figure 1 shows the surface distribution of the relative chemical fluxes of these termination steps for July 1750, 1970 and 2014 (enlargements over North America, Europe and Asia are in Supplementary Figs. 8–10).

In the pre-industrial era (1750), peroxyl-radical self-reactions (green) dominate. Biomass burning (forest fires) in Russia and Canada show termination by the uptake of HO_2 onto aerosol (blue), whereas fires over Kazakhstan show termination by OH + NO_2 (red) (Extended Data Fig. 1 shows a simulation with biomass burning switched off). This reflects the differing balance of NO_x relative to particulates emitted by different fires[16]. Desert dust makes only a limited contribution to the aerosol surface area, leading to some increased contribution of HO_2 uptake over Mauritania, Oman and Iran, but overall the impact is minor (Extended Data Fig. 1 shows a simulation with no desert dust emissions). Some HO_2 uptake by sea salt occurs over the northern Atlantic/Pacific and over the Arabian sea (Extended Data Fig. 1 shows a simulation with no sea-salt emissions).

In 1970, industrial and transport emissions over North America, Europe and Japan[17] have a profound impact on the radical termination processes. Many of the cities in North America, Europe and Japan are red, indicating NO_2 + OH as the dominant termination step. However, over Europe, large regions of the North Sea and eastern Germany are magenta (balance between OH + NO_2 and aerosol uptake), with much of eastern Europe being cyan (balance between peroxyl-radical self-reaction and aerosol uptake). Over North America, West Coast cities (Los Angeles, San Francisco and Seattle) show NO_2 + OH domination, while cities around the Great Lakes and those on the East Coast show large fractions of the radical termination being due to HO_2 uptake (magenta, cyan), reflecting the different industrial and transport sources in these regions. Most of Japan is red or yellow,

[1]Department of Chemistry, University of York, York, UK. [2]National Centre for Atmospheric Science, University of York, York, UK.
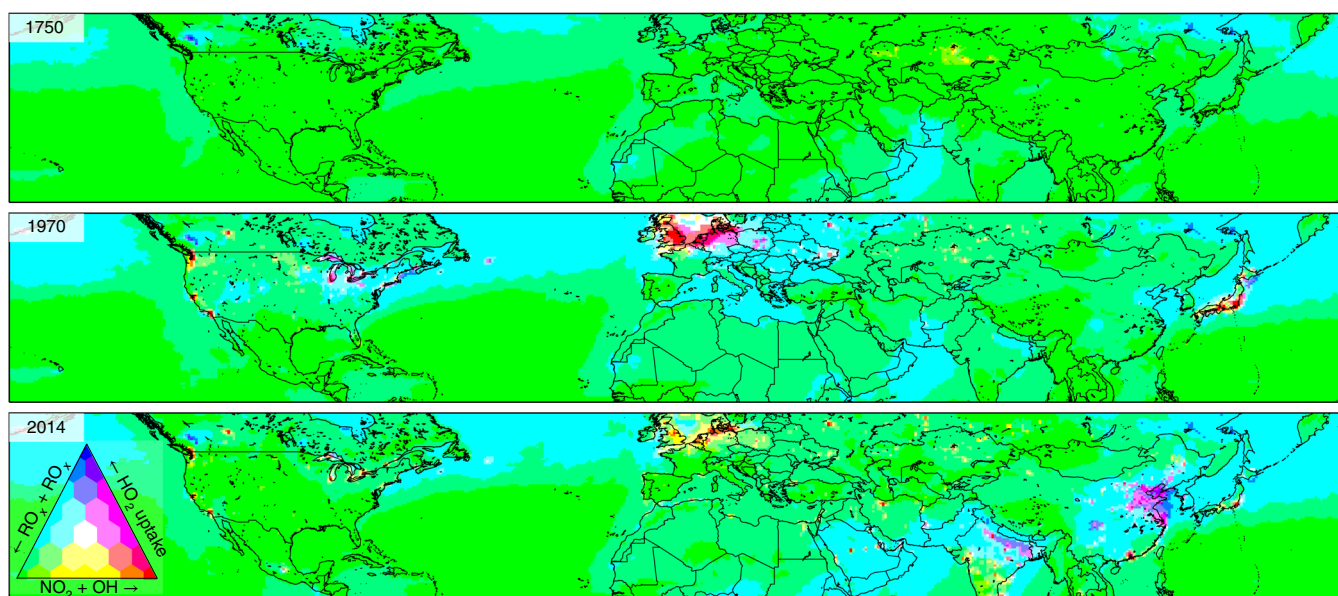✉e-mail: mat.evans@york.ac.uk

Fig. 1 | Map of the fractional contribution of each radical loss pathway for the years 1750, 1950 and 2014. Mean simulated July solar noon-time fraction of radical termination at the surface that occurs through OH + NO$_2$ (red), peroxyl-radical self-reactions (green) and aerosol uptake of HO$_2$ (blue) for 1750, 1970 and 2014. Enlargements of North America, Europe and Asia are shown in the Supplementary Information.

showing limited impact of HO$_2$ uptake. In 1970, China and India remain dominated by peroxyl-radical self-reaction, but there is some increased uptake of HO$_2$ by aerosols over populated regions relative to the pre-industrial era. Extensive areas of the oceans are cyan, indicating large HO$_2$ uptake. Some of this is driven by sea salt (Extended Data Fig. 1), but some is driven by shipping emissions (see Extended Data Fig. 2 without shipping emissions) and some by outflow of aerosol from industrial regions.

By 2014, the balance has changed as North America, Europe and Japan implemented policies to substantially reduce emissions of NO$_x$, VOCs, primary aerosols and aerosol precursors[17]. The relative importance of both OH + NO$_2$ and HO$_2$ uptake onto aerosols for termination has reduced, reflecting these emissions reductions. Over Asia, however, emissions have increased due to population growth and industrialization, leading to increases in NO$_x$ and PM concentrations. Large regions are now coloured magenta (balanced HO$_2$ uptake and OH + NO$_2$) or blue (dominated by HO$_2$ uptake).

This behaviour is seen predominantly within the boundary layer (Extended Data Fig. 3). In regions with more active mixing between the surface and the mid-troposphere, uptake onto aerosols can remain regionally important at 800 hPa, and NO$_2$ + OH can be important over cities. In general, the importance of these regimes decreases through the atmosphere so that at 500 hPa, the atmosphere is dominated by peroxyl-radical self-reactions. At higher altitudes, lightning NO$_x$ can lead to an increase in the importance of NO$_2$ + OH as a termination process.

Photochemical regimes

Figure 2 splits the domain based on the local largest termination step (enlarged versions for North America, Europe and Asia are in Supplementary Figs. 11–13). At a global scale, most locations are in an NO$_x$-limited regime (green), with some cities in a VOC-limited (red) regime. However, for large regions, the uptake of HO$_2$ onto aerosol (blue) is the largest termination reaction, and thus they do not fall into either of the two classically applied policy-control regimes. We call this third regime 'aerosol inhibited' as the presence of aerosols inhibits the formation of O$_3$ on short photochemical timescales. Area- and population-weighted

fractions over differing regions for the three regimes are given in Supplementary Tables 1 and 2.

As with the radical loss plot (Fig. 1), in 1750 the world was dominated by radical self-reactions, and so, except for forest-fire locations, the world was entirely NO$_x$ limited. In the 1970s, the large North American cities, northern Europe and southern Japan had become VOC limited. Although not recognized at the time, aerosol-inhibited regimes existed in regions downwind of these VOC-limited environments (eastern seaboard of the United States, Poland, downwind of Japan) and in some remote locations impacted by desert dust and shipping. In 1970, around 30% of the populations of Europe and North America and 71% of the population of Japan lived in VOC-limited regions, but only a small portion (<10%) lived in an aerosol-inhibited regime. Negligible fractions lived in that regime in the rest of the Northern Hemisphere.

By 2014, the success of air-quality strategies meant that aerosol-inhibited regimes over Europe and North America had mostly disappeared, leaving behind some relatively polluted city regions as VOC limited, but with most people living in NO$_x$-limited regions (80% in Europe and North America, 66% in Japan). However, industrialization in Asia moved many cities to be VOC limited (19% in China and 11% in India), but much larger populations in those regions live in aerosol-inhibited regions (36% and 39%, respectively), notably, in the Indo-Gangetic Plain and eastern China. The aerosol-inhibited regime plays a more important role in Asia in 2014 than it did in Europe and North America in 1970.

Understanding of the chemistry in this new third photochemical regime is still poor. The reactive uptake coefficient for HO$_2$ on aerosol (γ_{HO_2}) can vary by orders of magnitude depending on relative humidity, aerosol composition and the concentration of transition metals[12,18–21]. The work here assumes a uniform γ_{HO_2} of 0.2, consistent with previous modelling work[13]. Simulations run with a γ_{HO_2} of 0.1 still lead to regions in the aerosol-inhibited regime (Extended Data Fig. 4), but the fraction of the population living in this regime reduces (9% of China and 5% of India). A reduction in the γ_{HO_2} to 0.05 results in some areas still being within the regime, but these are now restricted to coastal Chinese regions. A γ_{HO_2} of less than 0.05 as suggested by some early studies[20] would probably
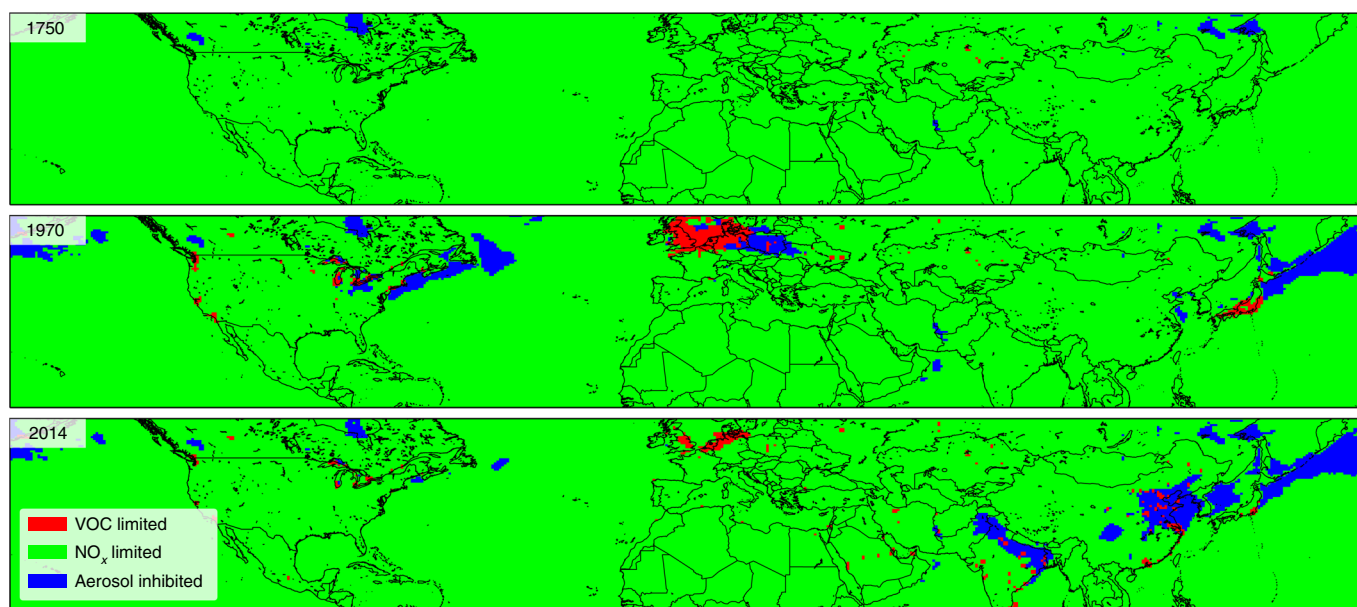
Fig. 2 | Map of the photochemical ozone-control regime for the years 1750, 1950 and 2014. Mean simulated July solar noon-time photochemical ozone-control regime for 1750, 1970 and 2014. Enlargements of North America, Europe and Asia are shown in the Supplementary Information.

result in very few locations being in the aerosol-inhibited regime. Thus with our model, this new photochemical regime exists for γ_{HO2} greater than 0.05 and is probably important for values greater than 0.1. Field observations of radicals in the aerosol-inhibited regions are rare. Observations and box modelling made in central Beijing[22] show a VOC-limited regime consistent with the modelling here, with similar conclusions for central New Delhi[23]. Observations from a more remote site in the North China Plain[24] suggest an NO_x-limited regime, whereas the modelling here would suggest an aerosol-limited one for that location. Reducing the γ_{HO2} to 0.1 would give a consistent response here. Another area little explored is the ability to simulate aerosol surface-area density in models (Supplementary Fig. 7). Mass of particulate matter less than 2.5 μm in diameter (PM2.5) is often evaluated in models since it is the primary health metric and more readily observable[25], and sometimes aerosol number density is evaluated because of its important role in light scattering and cloud–aerosol interaction[26], but systematic evaluations of modelled aerosol surface area are rare.

Impact on O_3

The additional radical sink offered by the uptake of HO_2 onto aerosol has a profound effect on regional O_3 concentrations. Figure 3 shows the impact on O_3 concentrations of switching off the uptake of HO_2 onto aerosol ($\gamma_{HO2} = 0$). In the pre-industrial 1750 simulation, the reactive uptake of HO_2 onto aerosols has a small impact on O_3 concentrations (<2%). The only places where increases in O_3 can be seen is over the biomass-burning regions of Canada and Russia.

In 1970, industrialized regions of North America, Europe and Japan show larger impacts. Substantial increases in O_3 concentrations are seen in northern Germany (28%), Tokyo (18%) and the American Great Lakes (20%). Los Angeles displays the largest impact, resulting in a 35% increase in O_3 concentrations when HO_2 uptake is switched off. The O_3 changes over India and China in 1970 were less than 5%. Thus, for many parts of North America, Europe and Japan in the 1970s, particulate pollution enhanced the uptake of HO_2 onto aerosols and reduced O_3 pollution.

By 2014, O_3 sensitivity to HO_2 uptake had reduced in Europe, North America and Japan as policy interventions had reduced particulate-matter concentrations. Removing HO_2 uptake in those simulations leads to less than a 5% increase in O_3 concentrations.

Over China, however, removing the uptake of HO_2 onto aerosol increases O_3 concentrations in the North China plain by between 20% and 30%. Even higher values (>35%) can be seen over the Bohai and Yellow seas. An additional hot spot can be seen inland over Chengdu. The Indo-Gangetic Plain has some of the highest observed sensitivity globally, with O_3 increases of greater than 30%. Uptake of HO_2 within the model thus has a large influence on surface O_3 concentration, notably in present-day China and India.

Discussion

Although we have identified regions that are aerosol inhibited from a fast photochemical perspective, aerosols can have an impact on O_3 production more widely through a number of processes: other heterogeneous reactions[27,28], changes to photolysis rates[29] and changes to the boundary layer[30]. Thus, although the area might be aerosol inhibited from a radical perspective, the overall impact of a change of aerosol concentration may be more complicated.

Future work is necessary to better evaluate modelled aerosol surface area and to create a robust parameterization for γ_{HO2}. It would also be useful to have observational data in regions outside of large cities but subject to high particulate pollution as these are the areas influenced by the new regime. The existence, however, of a third aerosol-inhibited photochemical ozone regime, which currently covers large regions and populations in China and India, highlights the complexity of implementing policies to improve air quality. Strategies that focus on reducing particulate matter alone create a trade-off with increases in surface ozone, a phenomenon observed in China[13,31]. A simulation (Methods) over India, where the 2014 emissions of anthropogenic particulate precursors (SO_2, black carbon, organic carbon and dust) and biomass burning are halved (representing an aggressive air-quality intervention) leads to reduced particle surface-area densities (Extended Data Fig. 5) and increased O_3 concentrations (Extended Data Fig. 6). To counter this adverse outcome, policy development must account for the aerosol-inhibited regime and include contemporaneous reductions in other anthropogenic emissions. Figure 4 shows the fractional reductions in anthropogenic NO_x emissions that are necessary to mitigate the additional O_3 that would form from this aerosol emissions reduction. For a large part of the Indo-Gangetic plain, large (∼40%) parallel reductions in NO_x emissions would be needed to
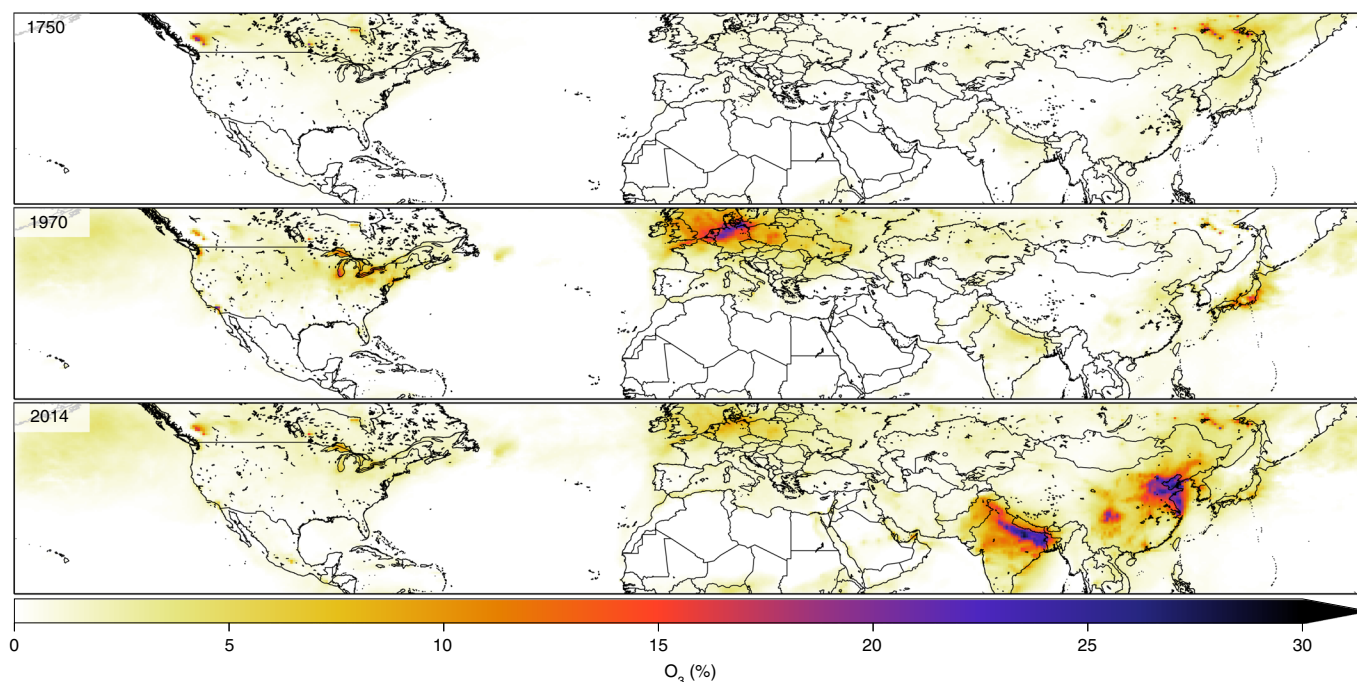
Fig. 3 | Map of the percentage increase in ozone concentration when uptake of HO$_2$ is switched off for 1750, 1970 and 2014. Percentage increase in monthly mean solar 15:00 LT O$_3$ concentration for July when heterogeneous uptake of HO$_2$ on aerosols is switched off for 1750, 1970 and 2014.
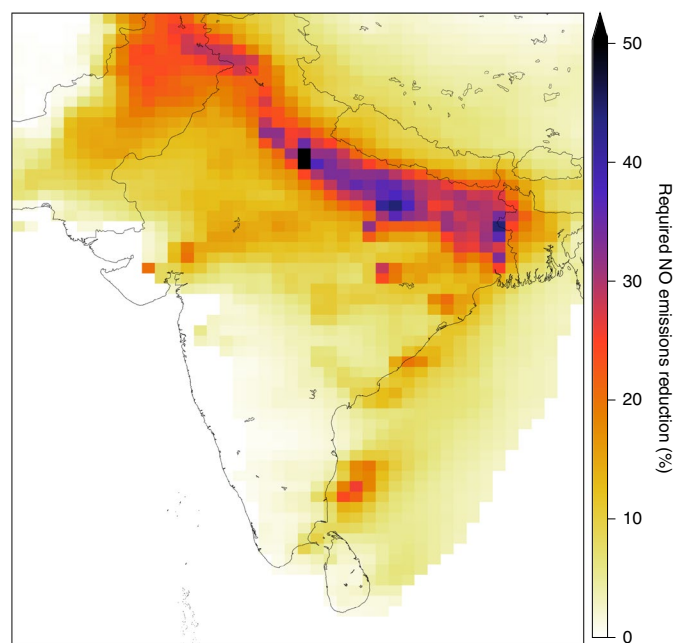

Fig. 4 | Map of fractional NO$_x$ emissions decrease required to offset a 50% reduction in aerosol emissions. Fractional decrease in 2014 NO$_x$ emissions that is necessary to offset the increase in surface, monthly mean and solar 15:00 LT O$_3$ caused by a 50% reduction in emissions of aerosol precursors (anthropogenic SO$_2$, black carbon, organic carbon, dust and all biomass-burning emissions).

stop O$_3$ concentrations from increasing. Although the direct health gains of reducing particulate-matter emissions will probably outweigh the disbenefits on health from increasing O$_3$ concentrations, there would probably be additional negative impacts on ecosystems, crop yield reductions and regional climate warming that would arise if aerosol-inhibition effects were not managed.

Online content

Any methods, additional references, Nature Research reporting summaries, source data, extended data, supplementary information, acknowledgements, peer review information; details of author contributions and competing interests; and statements of data and code availability are available at https://doi.org/10.1038/s41561-022-00972-9.

References

1. Fowler, D. et al. *Ground-Level Ozone in the 21st Century: Future Trends, Impacts and Policy Implications* (The Royal Society, 2008).
2. IPCC *Climate Change 2014: Synthesis Report* (eds Core Writing Team, Pachauri, R. K. & Meyer, L. A.) (IPCC, 2014).
3. Council, N. R. *Rethinking the Ozone Problem in Urban and Regional Air Pollution* (National Academies Press, 1991).
4. Sillman, S. The relation between ozone, NO$_x$ and hydrocarbons in urban and polluted rural environments. *Atmos. Environ.* **33**, 1821–1845 (1999).
5. Thornton, J. A. et al. Ozone production rates as a function of NO$_x$ abundances and HO$_x$ production rates in the Nashville urban plume. *J. Geophys. Res. Atmos.* **107**, 4146 (2002).
6. Sillman, S. & He, D. Y. Some theoretical results concerning O$_3$–NO$_x$–VOC chemistry and NO$_x$–VOC indicators. *J. Geophys. Res. Atmos.* **107**, 4659 (2002).
7. Lelieveld, J. et al. Atmospheric oxidation capacity sustained by a tropical forest. *Nature* **452**, 737–740 (2008).
8. Jacob, D. J. Heterogeneous chemistry and tropospheric ozone. *Atmos. Environ.* **34**, 2131–2159 (2000).
9. Read, K. A. et al. Extensive halogen-mediated ozone destruction over the tropical Atlantic Ocean. *Nature* **453**, 1232–1235 (2008).
10. Bey, I. et al. Global modeling of tropospheric chemistry with assimilated meteorology: model description and evaluation. *J. Geophys. Res. Atmos.* **106**, 23073–23095 (2001).
11. Martin, R. V., Jacob, D. J., Yantosca, R. M., Chin, M. & Ginoux, P. Global and regional decreases in tropospheric oxidants from photochemical effects of aerosols. *J. Geophys. Res. Atmos.* **108**, 4097 (2003).

12. Song, H. et al. Influence of aerosol copper on HO_2 uptake: a novel parameterized equation. *Atmos. Chem. Phys.* **20**, 15835–15850 (2020).

13. Li, K. et al. A two-pollutant strategy for improving ozone and particulate air quality in China. *Nat. Geosci.* **12**, 906–910 (2019).

14. Sakamoto, Y. et al. Relative and absolute sensitivity analysis on ozone production in Tsukuba, a city in Japan. *Environ. Sci. Technol.* **53**, 13629–13635 (2019).

15. Song, H. et al. Reduced aerosol uptake of hydroperoxyl radical may increase the sensitivity of ozone production to volatile organic compounds. *Environ. Sci. Technol. Lett.* **9**, 22–29 (2022).

16. Giglio, L., Randerson, J. T. & van der Werf, G. R. Analysis of daily, monthly, and annual burned area using the fourth-generation global fire emissions database (GFED4). *J. Geophys. Res. Biogeosci.* **118**, 317–328 (2013).

17. Hoesly, R. M. et al. Historical (1750–2014) anthropogenic emissions of reactive gases and aerosols from the Community Emissions Data System (CEDS). *Geosci. Model Dev.* **11**, 369–408 (2018).

18. Cooper, P. L. & Abbatt, J. P. D. Heterogeneous interactions of OH and HO_2 radicals with surfaces characteristic of atmospheric particulate matter. *J. Phys. Chem.* **100**, 2249–2254 (1996).

19. Thornton, J. A., Jaegle, L. & McNeill, V. F. Assessing known pathways for HO_2 loss in aqueous atmospheric aerosols: regional and global impacts on tropospheric oxidants. *J. Geophys. Res, Atmos.* **113**, D05303 (2008).

20. Macintyre, H. L. & Evans, M. J. Parameterisation and impact of aerosol uptake of HO_2 on a global tropospheric model. *Atmos. Chem. Phys.* **11**, 10965–10974 (2011).

21. Zhou, J. et al. Kinetics and impacting factors of HO_2 uptake onto submicron atmospheric aerosols during the 2019 air quality study (aquas) in Yokohama, Japan. *Atmos. Chem. Phys.* **21**, 12243–12260 (2021).

22. Whalley, L. K. et al. Evaluating the sensitivity of radical chemistry and ozone formation to ambient VOCs and NO_x in Beijing. *Atmos. Chem. Phys.* **21**, 2125–2147 (2021).

23. Nelson, B. S. et al. In situ ozone production is highly sensitive to volatile organic compounds in Delhi, India. *Atmos. Chem. Phys.* **21**, 13609–13630 (2021).

24. Tan, Z. F. et al. No evidence for a significant impact of heterogeneous chemistry on radical concentrations in the North China plain in summer 2014. *Environ. Sci. Technol.* **54**, 5973–5979 (2020).

25. Mortier, A. et al. Evaluation of climate model aerosol trends with ground-based observations over the last 2 decades—an AeroCom and CMIP6 analysis. *Atmos. Chem. Phys.* **20**, 13355–13378 (2020).

26. Fanourgakis, G. S. et al. Evaluation of global simulations of aerosol particle and cloud condensation nuclei number, with implications for cloud droplet formation. *Atmos. Chem. Phys.* **19**, 8591–8617 (2019).

27. Dentener, F. & Crutzen, P. J. Reaction of H_2O_5 on tropospheric aerosols: impact on the global distributions of NO_x, O_3, and OH. *J. Geophys. Res. Atmos.* **98**, 7149–7163 (1993).

28. Kleffmann, J., Becker, K. & Wiesen, P. Heterogeneous NO_2 conversion processes on acid surfaces: possible atmospheric implications. *Atmos. Environ.* **32**, 2721–2729 (1998).

29. He, S. & Carmichael, G. R. Sensitivity of photolysis rates and ozone production in the troposphere to aerosol properties. *J. Geophys. Res. Atmos.* **104**, 26307–26324 (1999).

30. Jacobson, M. Z. Studying the effects of aerosols on vertical photolysis rate coefficient and temperature profiles over an urban airshed. *J. Geophys. Res. Atmos.* **103**, 10593–10604 (1998).

31. Ma, Z. et al. Significant increase of surface ozone at a rural site, north of eastern China. *Atmos. Chem. Phys.* **16**, 3969–3977 (2016).

Methods

Model. GEOS-Chem[10] version 12.8 (http://www.geos-chem.org) was run in the tropchem configuration, which consists of 536 gas-phase, 76 heterogeneous and 133 photolytic reactions. Within the stratosphere, a linearized chemistry is used[32].

The same meteorology was used for each simulation, but anthropogenic emissions were varied on the basis of the Community Emissions Data System[17] emissions for 1750, 1970 and 2014 (the last available year). For each emissions year, the model was run globally at 4° × 5° for two years with the first year considered as spin-up. Boundary conditions and initial conditions were generated from the second year of simulation. These were then used in a one-month (1 June to 31 June) 1.00° × 1.25° nested simulation over a domain of 10° to 60° N latitude and 170° W to 170° E longitude to provide initial conditions for a final 0.500° × 0.625° simulation (1 July to 31s July) run over the same domain. The concentrations of all species within the chemistry scheme were archived each model time step from the high-resolution simulation, and these were then used to calculate chemical fluxes.

The GEOS-FP (forward processing) meteorological fields from the NASA Global Modelling and Assimilation Office (https://gmao.gsfc.nasa.gov/) drove model transport. All simulations used 47 vertical levels extending from the surface to approximately 80 km in altitude.

Other emissions were kept the same in all simulations: the MEGAN[33] inventory provided the biogenic emissions, GFED4[16] provided the biomass-burning emissions and DEAD[34] provided the dust emissions.

Loss rates. Chain-reaction termination rates were calculated offline from the archived species concentrations, physical parameters (temperature, pressure and humidity), aerosol parameters (component surface areas and radii) and the model rate constants.

We do not count the production of radical products in the peroxyl-radical self-reaction as termination steps but do assume that non-radical products are long lived on the timescale of the calculation and so offer a chain termination step.

The heterogeneous radical loss rate of HO_2 was calculated by iterating over the radius and surface area of each type of aerosol (organic carbon, black carbon, dust, sea salt, nitrate–sulfate–ammonium and secondary organic aerosol). These parameters were used in conjunction with temperature and air density to calculate the first-order HO_2 loss rate.

We calculate the flux through each chemical termination route at local solar noon for each grid box for each day of July and sum. We divide the individual monthly sums for each termination process by the total of the three termination processes over the month to derive the fractions shown.

Following ref. [6], we define a grid box's O_3 control regime by the largest of the three termination route.

HO_2 uptake coefficient. We have used a default HO_2 reactive uptake coefficient (γ_{HO2}) of 0.2 (ref. [8]). Laboratory studies using pure synthetic aerosol have found relatively low ($\gamma_{HO2} < 0.2$) values of uptake coefficients[18,35–37]; however, studies on real-world aerosol have found greater coefficients ranging from 0.08 to 0.40 (refs. [21,38,39]). It is likely that minor components of the aerosol such as transition metals may play an important role in this. Some evidence suggests copper appears to greatly enhance the uptake coefficients[40–42], and this has been shown to be present in Asian aerosol[43–45].

We run simulations where the γ_{HO2} is reduced to 0.1, 0.05 and 0.00 and show results in Extended Data Fig. 4. We treat H_2O as the sole product formed during the heterogeneous uptake of HO_2[46], but our conclusions do not change if we assume production of H_2O_2.

The use of a single value of γ_{HO2} is unlikely to be realistic. However, current parameterizations do not reproduce the observed temporal variability in γ_{HO2} (ref. [21]). Further study will be needed to provide an appropriate parameterization for γ_{HO2}. How the value of γ_{HO2} varies with the changing concentration of NO_x and radicals is likely to play an important role in determining the importance of HO_2 uptake for controlling O_3 concentrations.

Indian particulate emissions reductions. Over a more limited Indian domain (3° to 36° N latitude and 63° to 94° E longitude), we repeat the July 2014 simulation at 0.25° by 0.3125°. We then half the 2014 emissions of anthropogenic particulate precursors (SO_2, black carbon, organic carbon and anthropogenic dust) and all biomass-burning emissions to simulate an aggressive local effort to reduce particulate-matter pollution. This reduces particulate surface-area densities substantially (Extended Data Fig. 5) and leads to increased O_3 concentrations (Extended Data Fig. 6). With the reduced particulate-matter emissions, we then run five simulations reducing anthropogenic NO_x emissions by 10%, 20%, 30%, 40% and 50%. For each surface model grid box, we fit a third-order polynomial through a graph of monthly mean 15:00 LT O_3 concentration against the percentage NO_x reduction and identify when the value of NO_x emissions reduction gives the same mean O_3 concentration as in the simulation without any reduction in particulate-matter emissions. This value of NO_x reduction is then plotted for each grid box as in Fig. 4.

Data availability

All data used to produce this paper are available at https://doi.org/10.5285/406f88e e14f34177934b1dbd0be6aac7.

Code availability

The GEOS-Chem model is available from https://github.com/geoschem/geos-chem. Code used to draw up the figures in the paper are deposited alongside the data.

References

32. Eastham, S. D., Weisenstein, D. K. & Barrett, S. R. H. Development and evaluation of the unified tropospheric–stratospheric chemistry extension (UCX) for the global chemistry-transport model GEOS-Chem. *Atmos. Environ.* **89**, 52–63 (2014).
33. Guenther, A. B. et al. The Model of Emissions of Gases and Aerosols from Nature version 2.1 (MEGAN2.1): an extended and updated framework for modeling biogenic emissions. *Geosci. Model Dev.* **5**, 1471–1492 (2012).
34. Fairlie, T., Jacob, D. & Park, R. The impact of transpacific transport of mineral dust in the United States. *Atmos. Environ.* **41**, 1251–1266 (2007).
35. Hanson, D. R., Burkholder, J. B., Howard, C. J. & Ravishankara, A. R. Measurement of OH and HO_2 radical uptake coefficients on water and sulfuric-acid surfaces. *J. Phys. Chem.* **96**, 4979–4985 (1992).
36. Gershenzon, Y. M., Grigorieva, V. M., Ivanov, A. V. & Remorov, R. G. O_3 and OH sensitivity to heterogeneous sinks of HO_x and CH_3O_2 on aerosol particles. *Faraday Discuss.* **100**, 83–100 (1995).
37. Matthews, P. S. J., Baeza-Romero, M. T., Whalley, L. K. & Heard, D. E. Uptake of HO_2 radicals onto Arizona test dust particles using an aerosol flow tube. *Atmos. Chem. Phys.* **14**, 7397–7408 (2014).
38. Taketani, F. et al. Measurement of overall uptake coefficients for HO_2 radicals by aerosol particles sampled from ambient air at mts. Tai and Mang (China). *Atmos. Chem. Phys.* **12**, 11907–11916 (2012).
39. Zhou, J., Murano, K., Kohno, N., Sakamoto, Y. & Kajii, Y. Real-time quantification of the total HO_2 reactivity of ambient air and HO_2 uptake kinetics onto ambient aerosols in Kyoto (Japan). *Atmos. Environ.* **223**, 117189 (2020).
40. Lakey, P. S. J., George, I. J., Baeza-Romero, M. T., Whalley, L. K. & Heard, D. E. Organics substantially reduce HO_2 uptake onto aerosols containing transition metal ions. *J. Phys. Chem. A* **120**, 1421–1430 (2016).
41. Thornton, J. & Abbatt, J. P. D. Measurements of HO_2 uptake to aqueous aerosol: mass accommodation coefficients and net reactive loss. *J. Geophys. Res. Atmos.* **110**, D08309 (2005).
42. Taketani, F., Kanaya, Y. & Akimoto, H. Kinetics of heterogeneous reactions of HO_2 radical at ambient concentration levels with $(NH_4)(2)SO_4$ and NaCl aerosol particles. *J. Phys. Chem. A* **112**, 2370–2377 (2008).
43. Schroeder, W. H., Dobson, M., Kane, D. M. & Johnson, N. D. Toxic trace elements associated with airborne particulate matter: a review. *J. Air Waste Manage. Assoc.* **37**, 1267–1285 (1987).
44. Allen, A. G., Nemitz, E., Shi, J. P., Harrison, R. M. & Greenwood, J. C. Size distributions of trace metals in atmospheric aerosols in the United Kingdom. *Atmos. Environ.* **35**, 4581–4591 (2001).
45. Ross, H. B. & Noone, K. J. A numerical investigation of the destruction of peroxy radical by Cu ion catalysed reactions on atmospheric particles. *J. Atmos. Chem.* **12**, 121–136 (1991).
46. Mao, J., Fan, S., Jacob, D. J. & Travis, K. R. Radical loss in the atmosphere from Cu–Fe redox coupling in aerosols. *Atmos. Chem. Phys.* **13**, 509–519 (2013).

Author contributions

P.D.I., M.J.E. and A.C.L. contributed to generating the ideas, methodology and writing. P.D.I. ran the simulations, adapted the model and generated the figures.

Competing interests

The authors declare no competing interests.

Additional information

Extended data is available for this paper at https://doi.org/10.1038/s41561-022-00972-9.

Supplementary information The online version contains supplementary material available at https://doi.org/10.1038/s41561-022-00972-9.

Correspondence and requests for materials should be addressed to Mathew J. Evans.

Peer review information *Nature Geoscience* thanks Keding Lu and the other, anonymous, reviewer(s) for their contribution to the peer review of this work. Primary Handling Editors: Xujia Jiang and Thomas Richardson, in collaboration with the *Nature Geoscience* team

**Reprints and permissions information** is available at www.nature.com/reprints.
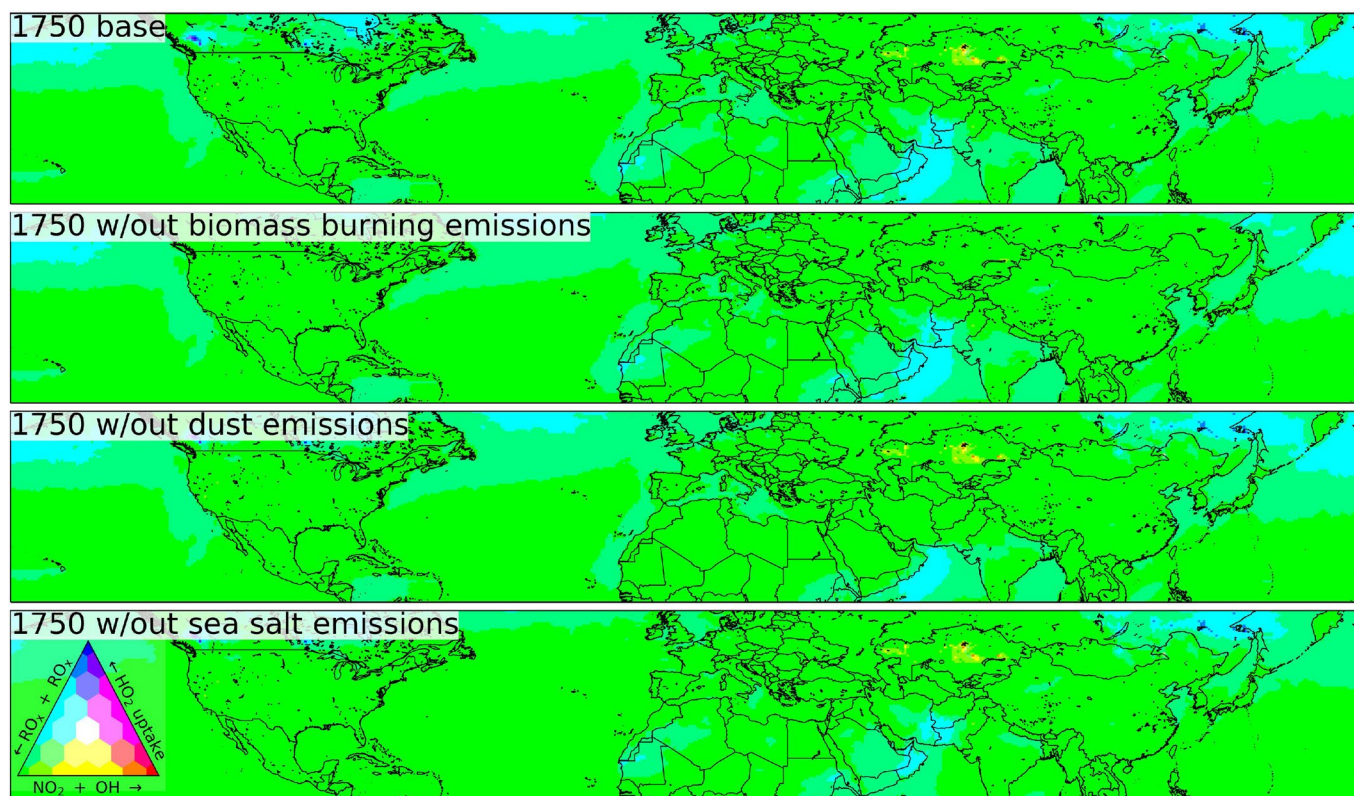
Extended Data Fig. 1 | Map of the fractional contribution of radical loss pathways under different 1750 emission scenarios. Average simulated July noon-time fraction of radical termination at the surface that occurs through the OH + NO$_2$, peroxy radical self-reactions and aerosol uptake of HO$_2$ for 1750 in the base model, without any biomass burning, without any desert dust emissions, and without any sea salt emissions.
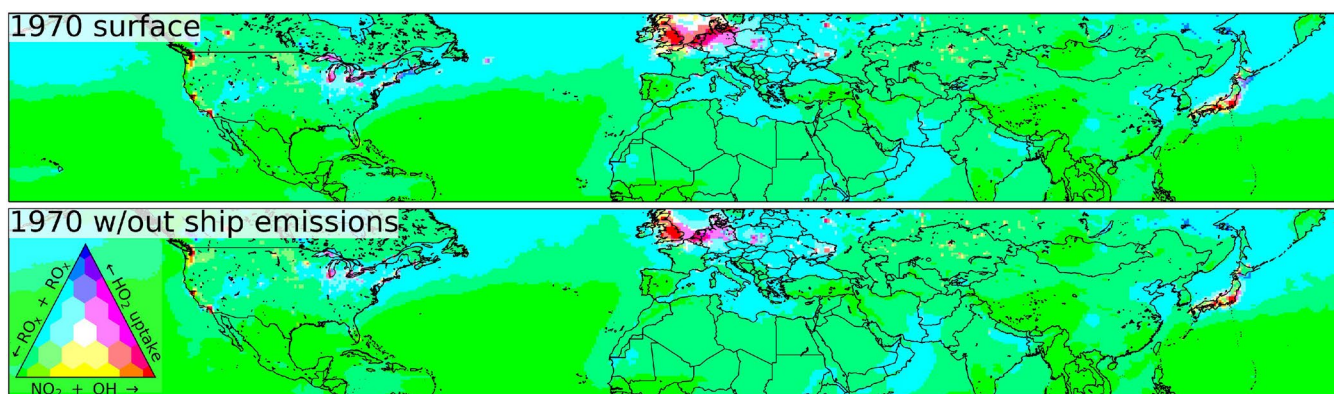
Extended Data Fig. 2 | Map of the fractional contribution of radical loss pathways with and without shipping emissions in 1970. Average simulated July noon-time fraction of radical termination at the surface that occurs through the OH + NO$_2$, peroxy radical self-reactions and aerosol uptake of HO$_2$ for 1970 in the model with and without shipping emissions.
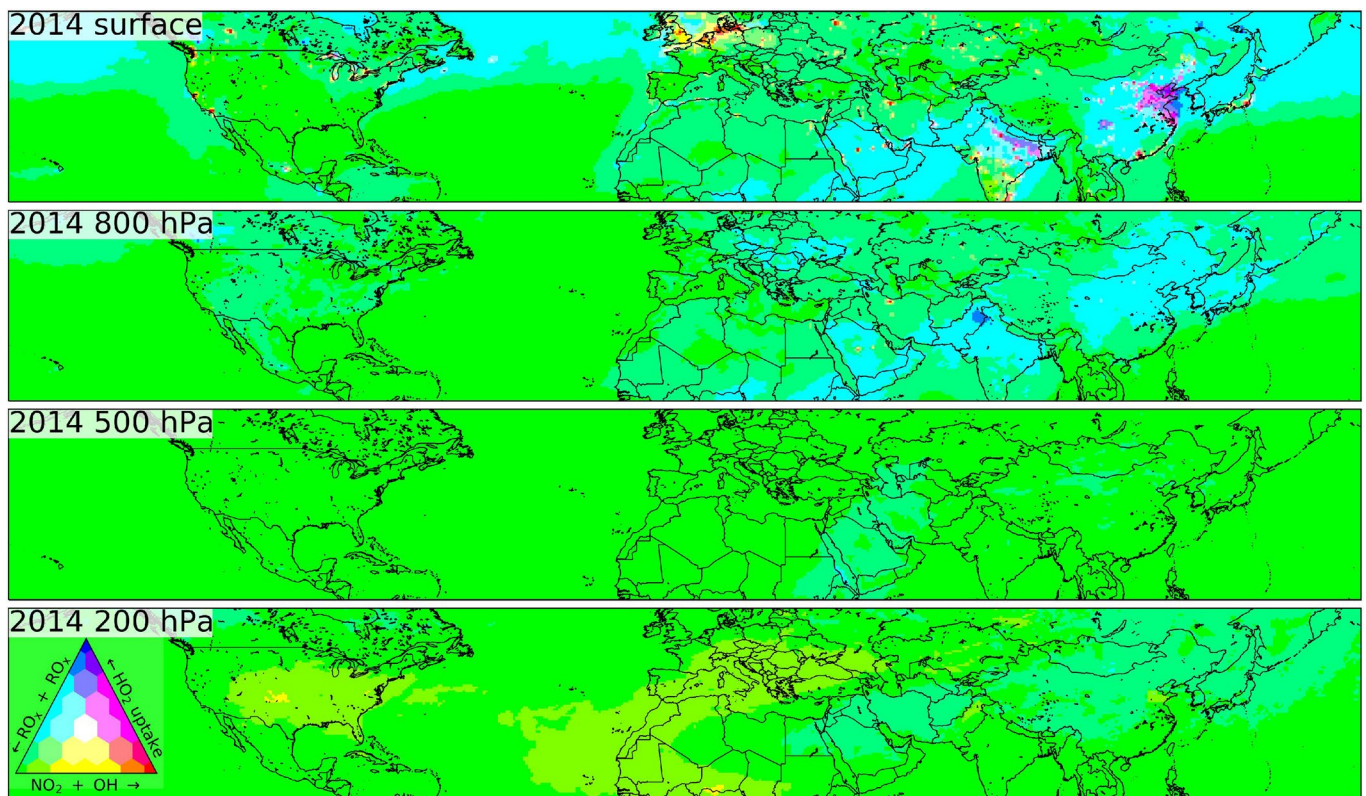
Extended Data Fig. 3 | Fractional contribution of radical loss pathways in 2014 at different altitudes. Average simulated July noon-time fraction of radical termination that occurs through the OH + NO_2, peroxy radical self-reactions and aerosol uptake of HO_2 at the surface, 800 hPa, 500 hPa and 200 hPa.
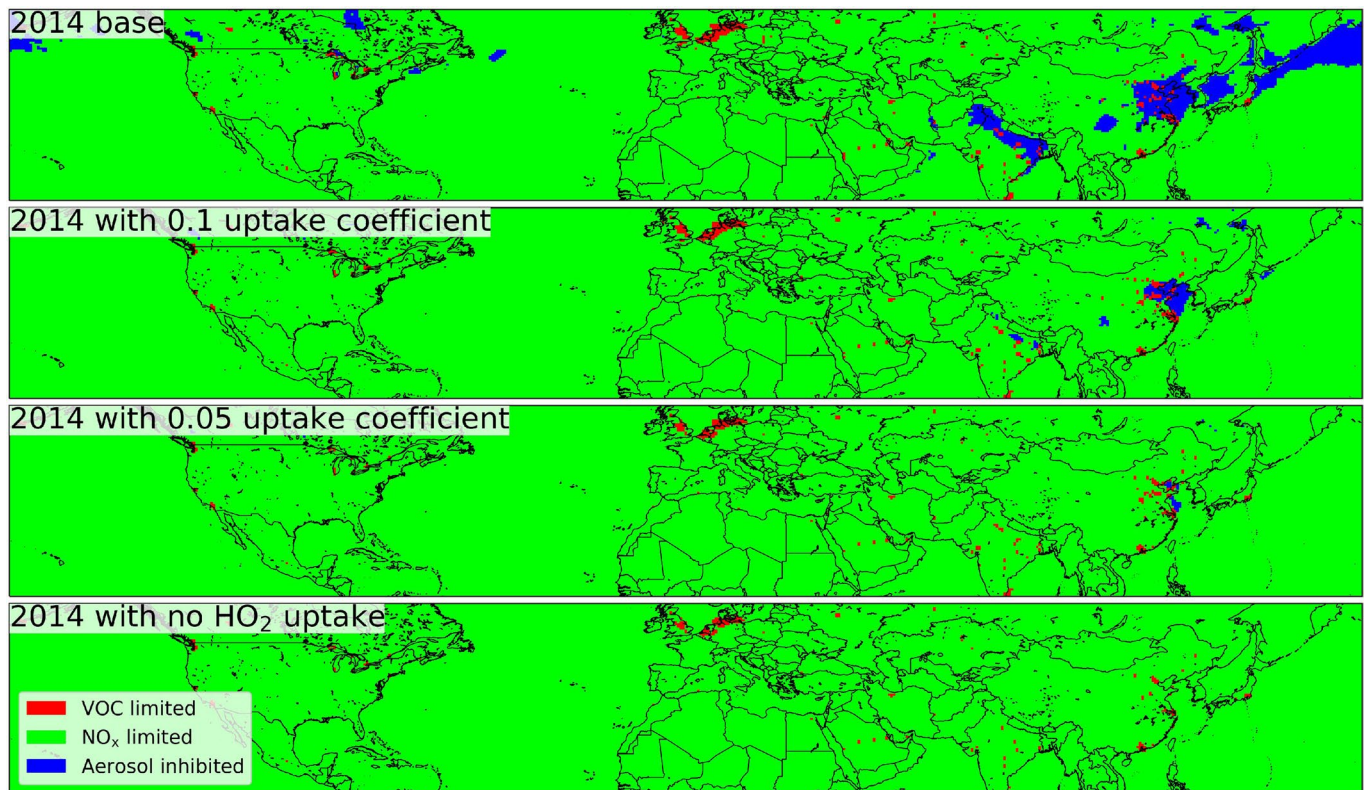
Extended Data Fig. 4 | Map of the fractional contribution of radical loss pathways in 2014 with different HO$_2$ uptake coefficients. Average simulated July noon-time photochemical regime in 2014 with γ_{HO2} of 0.2 (base), 0.1, 0.05 and 0.0.
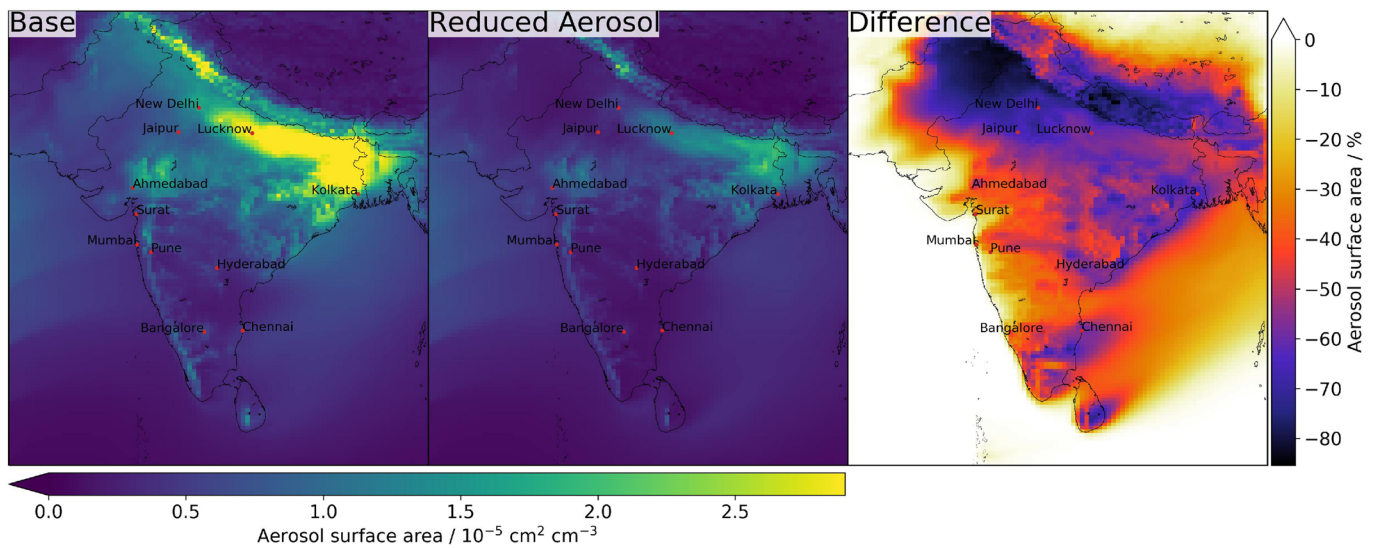
Extended Data Fig. 5 | Map of a 50% reduction in aerosol emissions in India. July 2014 mean surface aerosol surface area density over India in a base simulation and in a simulation with a 50% reduction in emission of aerosol precursors (anthropogenic SO_2, black carbon, organic carbon, dust, and all biomass burning emissions).
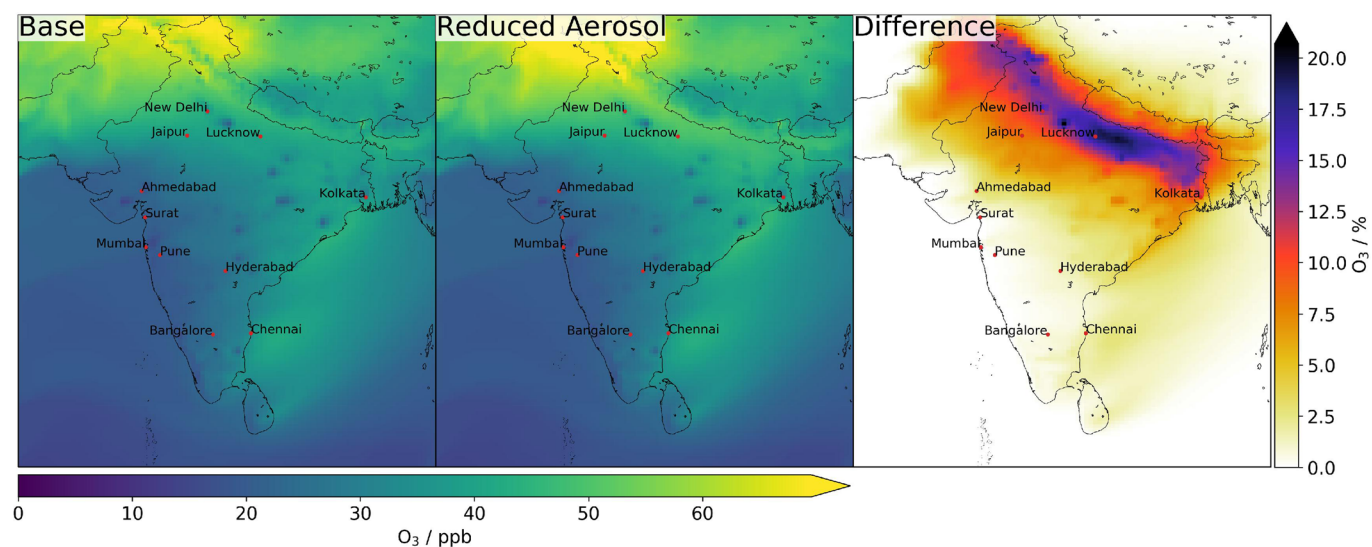
Extended Data Fig. 6 | Map of the ozone change with a 50% reduction in aerosol emissions in India. July 2014 mean O_3 mixing ratios over India in a base simulation and in a simulation with a 50% reduction in emission of aerosol precursors (anthropogenic SO_2, black carbon, organic carbon, dust, and all biomass burning emissions).